

Databank of proton tracks in polyallyldiglycol carbonate (PADC) solid-state nuclear track detector for neutron energy spectrometry



D. Nikezic^{a,b}, B. Milenkovic^a, K.N. Yu^{b,*}

^a Faculty of Science, University of Kragujevac, R. Domanovica 12, Kragujevac 34000, Serbia

^b Department of Physics and Materials Science, City University of Hong Kong, Tat Chee Avenue, Kowloon, Hong Kong

ARTICLE INFO

Article history:

Received 29 June 2015

Received in revised form

18 August 2015

Accepted 27 August 2015

Available online 7 September 2015

Keywords:

Etched tracks

Recoiled protons

Neutrons

Polyallyldiglycol carbonate

PADC

Solid-state nuclear track detector

ABSTRACT

A computer program for studying etched proton tracks in the polyallyldiglycol carbonate (PADC) solid-state nuclear track detector was prepared. The program provided visualization of track appearance as seen under the optical microscope in the transmission mode. Measurable track parameters were also determined and displayed and written in a data file. Three-dimensional representation of tracks was also enabled. Application of this software in neutron dosimetry for energy up to 11 MeV was demonstrated through the creation of a databank with a large number of tracks, which would be used to compare real-life tracks obtained in the PADC detector upon neutron irradiation. One problem was identified, viz., very similar tracks were obtained from protons with very different energies and incident angles, and strategies to solve this were proposed.

© 2015 Elsevier B.V. All rights reserved.

1. Introduction

To estimate the equivalent dose from neutrons, it is necessary to involve the radiation weighting factors of neutrons, which in turn depend on the neutron energies. As such, it is of primary importance to explore methods to determine the neutron energy [1]. Recently we have studied the feasibility of neutron spectrometry with polyallyldiglycol carbonate (PADC) detectors (commercially available as CR-39 detectors), where some major problems in this research field were identified [2].

There are active methods for measuring the energy spectra for neutrons based on Bonner spheres or other devices [3,4]. However, in some applications, passive and long-term integrated measurements are needed. One example is the measurements of energy spectra for neutrons to determine the resulting dose in radiation treatment rooms installed with high-energy accelerators. Solid-state nuclear track detectors (SSNTDs) have emerged as a promising solution for this task, including the PADC film detector, which is one of the most commonly used SSNTDs [5–7]. There have been several attempts to measure neutron energy spectra with SSNTDs through studies on the parameters of openings of etched tracks [8–10]. Bare PADC detector was considered here, i.e.,

there were no converters in front of the detector. It is true that a converter (e.g., a polyethylene film) significantly increases the detector response in term of track density, but much information on neutron energies and their spectrum will be lost.

The most commonly used method for neutron detection using SSNTDs is through the studies on the recoiled protons, which are the product of elastic collision between neutrons and nuclei of hydrogen atoms. The neutron energy E_n , proton energy E_p and recoiled angle θ are related by the equation

$$E_p = E_n \cos^2 \theta. \quad (1)$$

The recoiled protons may have energies between 0 and E_n , and the probability distribution is uniform in this range. If the neutrons have a continuous energy spectrum, a variety of protons will be created. From the energies of the protons, it is possible to reconstruct the neutron energy spectrum through de-convolution procedures.

The track appearance under the optical microscope in the transmission mode depends on several parameters, e.g., the particle energy and the corresponding stopping power in the detector material, the incident angle with respect to the detector surface, the etching conditions and the removed layer during the etching, etc. As such, measurement of proton energy is possible through studies on their etched tracks in the PADC film detector. However, a variety of very different tracks can be produced in the detector

* Corresponding author. Tel.: +852 34427812; fax: +852 34420538.

E-mail addresses: nikezic@kg.ac.rs (D. Nikezic),

bmilenkovic@kg.ac.rs (B. Milenkovic), peter.yu@cityu.edu.hk (K.N. Yu).

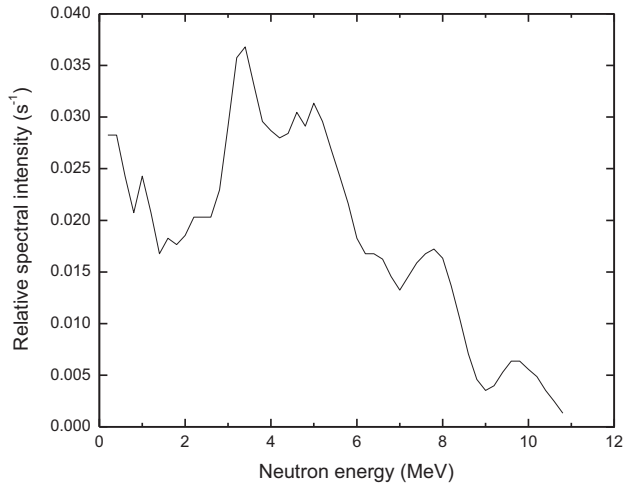


Fig. 1. Relative spectral intensity (s^{-1}) of neutrons emitted from an AmBe source [11].

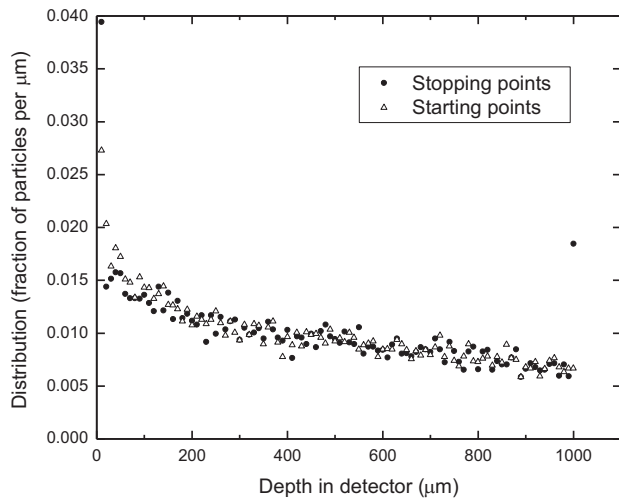


Fig. 2. Starting and stopping points of recoiled protons in a PADC film detector. The detector thickness was 1 mm. A significantly larger number of stopping points at a depth of 1000 μm corresponded to those protons which had left the detector on the opposite side. The distribution was given in (fraction of particles per μm). A total of 1000 events were presented in this figure.

and evaluation of the proton energy and the incident angle from the track appearance presents a challenging task.

When neutrons pass through the detector, they interact with the atomic nuclei in the detector through inelastic and elastic collisions. As a result of elastic collisions with nuclei of hydrogen atoms, recoiled protons are created within the body of the detector with various energies and directions. Creation of other recoiled nuclei (carbon and oxygen) is negligible in the energy range up to 11 MeV, which is considered here.

In laboratories, one of the most common neutron sources is the AmBe source. The energy spectrum of neutrons from this source, shown in Fig. 1 [11], is used to check our approach in determination of neutron spectra. In Fig. 2, the starting points (i.e., the points where elastic collisions take place to create recoil protons) and ending point of protons are shown. To obtain this figure, it was assumed that the PADC film detector was in contact with the AmBe source so all incident angles of neutrons onto the detector surface in π geometry were possible. One can notice from Fig. 2 that a large number of protons were “stopped” at 1000 μm (i.e., the point at 1000 μm was much higher than the adjacent point). In fact, this point represented those protons which escaped

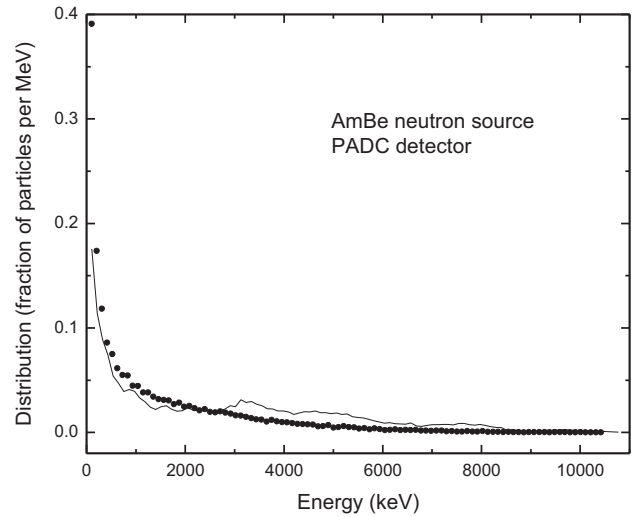


Fig. 3. Energy distributions of recoiled protons (scattered points) and of neutrons (line) which created the recoiled protons upon elastic collisions with hydrogen nuclei. The distribution was given in fraction of particles per MeV. The distribution was calculated using a Monte Carlo method.

from the detector from the opposite side. If the detector was immersed in an etchant, these escaped protons would lead to reversed etching [12], which would further complicate the measurements. In order to avoid this complication, one can mask the opposite side of the detector to prevent reversed etching. From Fig. 2, it is also clear that through etching away several micrometers of the detector, only a small fraction of tracks will be revealed. With prolonged etching, more and more tracks will be observed, while those which have been found earlier will have become progressively larger. Fig. 3 shows the energy distribution of neutrons which create recoiled protons, and the energy distribution of protons themselves. Calculations were again performed for the PADC film detector in contact with an AmBe neutron source.

It is remarked here that other interactions are also possible with the atomic nuclei in the PADC film detector, such as inelastic collisions which excite the atomic nuclei and lead to subsequent emission of beta and gamma radiations. Such interactions do not produce recoiled protons and do not leave latent tracks in the detectors, and as such they should be considered competitions when the absolute detector response is determined. From Figs. 2 and 3, it is clear that neutron interactions with the PADC film detector will produce proton latent tracks with different orientations, lengths and starting points.

2. Methodology

To facilitate the estimation of the proton energy from the track in PADC film detectors, we prepared a computer code which could be used to generate a databank of tracks showing their appearance under the optical microscope in the transmission mode. This databank could be further used to match the tracks obtained in real-life experiments to determine the proton energy and the incident angle. Some issues in such a matching procedure and in the determination of the proton and neutron energies will be discussed in the following.

The current computer program was developed based on our two previous computer codes, namely, TRACK_TEST and TRACK_VISION, which were developed exclusively for tracks generated by alpha-particle irradiation and subsequent chemical etching, which were important for radon dosimetry [13,14]. These computer

codes were modified to take into consideration the ranges of protons in PADC and also the corresponding V function of protons, where $V(R')=V_t/V_b$, R' is the residual range (i.e., the distance between a studied point on the etched track and the point in detector where the incident particle was stopped), V_t is the etch rate along the track and V_b is the etch rate of the bulk detector [5].

The ranges of protons in PADC were calculated using the freely available SRIM2003 software [15], which produced a table with data on the stopping powers and ranges as functions of the proton energy. The stoichiometric formula for the PADC detector was taken as $C_{12}H_{18}O_7$ and the density was taken as 1.32 g cm^{-3} . When compared with an alpha particle, a proton has half the electronic-charge value and one-fourth of the mass, and thus a much longer range in PADC. For example a proton with an energy of 10 MeV has a range of $\sim 952 \mu\text{m}$ in PADC, while an alpha particle with the same energy has a range of $\sim 85 \mu\text{m}$.

Another important difference between protons and alpha particles is their stopping powers in PADC, which determines the function $V(R')$. It has been shown that V is related to the restricted energy loss REL. However, a more convenient form for V is the empirical form shown in Eq. (2):

$$V(R') = 1 + [A_1 e^{-A_2 R'} + A_3 e^{-A_4 R'}] \cdot [1 - e^{-A_5 R'}]. \quad (2)$$

In the present work, the V function of protons in PADC was adopted from Ref. [16] in the form of Eq. (2), with the parameters $A_1=0.4306$, $A_2=7.3736 \times 10^{-3}$, $A_3=1.0559$, $A_4=0.1072$ and $A_5=1.4120$. Both the longer ranges and smaller V values for protons when compared to alpha particles led to different appearance of proton and alpha-particle tracks. An example of the 3-D representation of a proton track is shown in Fig. 4.

3. Examples of calculated tracks

As described in previous sections, in a real-life experiment on neutron measurements with the PADC detector, we can expect to obtain many etched tracks with different size, shape, gray levels under the optical microscope, etc., depending on the initial energy and incident angle of the recoiled protons, and the effective removed layer of the PADC film detector during etching. For

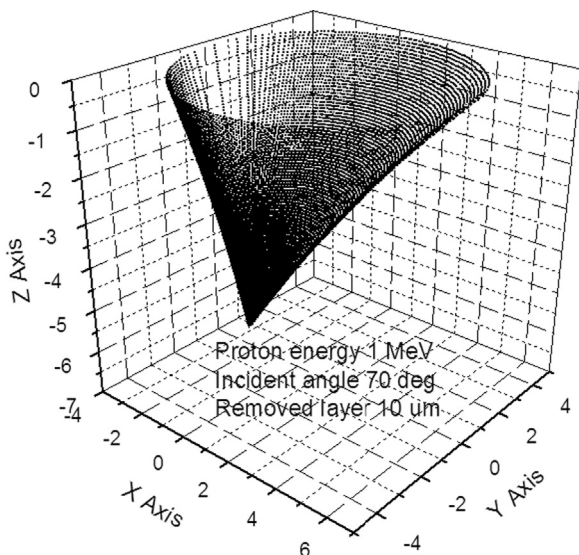


Fig. 4. A 3-D representation of a proton track. A total of 19800 points have been used to represent the track.

illustration purposes, some representative tracks which may be obtained from real-life experiments are shown in Fig. 5, where we have assumed that track development starts on the original detector surface. The tracks shown in Fig. 5 were generated by protons with energies between 0.5 and 5 MeV with incident angles of 90° , 70° and 50° , and corresponded to removed layers of 5 and $10 \mu\text{m}$. The parameters of the tracks are also shown in Fig. 5. These show that very different tracks can be found from neutron irradiation of the PADC detector.

4. Pattern recognition and determination of proton energy and incident angle

The task of determining the proton energy and incident angle from the track appearance (including size, gray level, major and minor axes, etc.) falls into the field of pattern recognition. In order to perform such pattern recognition in the track appearance, a large databank was created by calculations. In order to facilitate and accelerate the calculation, which was needed to create such file with large number of data, previous programs were looped and all graphical presentations were disabled. Track parameters, major and minor axes, and the fractions of the black portion in the tracks were determined by changing the proton energy between 0.1 and 11 MeV with steps of 0.1 MeV, by changing the incident angle between 20° and 90° (with 90° meaning normal incidence onto the detector surface) with steps of 2° , and by changing the removed layer between 1 and $50 \mu\text{m}$ with steps of $1 \mu\text{m}$. These data were stored in the file DATABANK.DAT.

The next step was to simulate the irradiation of PADC detector with neutrons from an AmBe source assuming normal incidence of neutrons onto the detector surface. Normal incidence could be achieved in real-life experiments, e.g., if the detector was located at a sufficiently large distance from the source. The recoiled protons were created at different depths within the detector with various energies and incident angles. For illustration purposes, the removed layer of the detector was taken to be $20 \mu\text{m}$ during etching, and the parameters of about 1040 tracks were computed. The parameters of these tracks were stored in another file. The energy and incident angle of the recoiled protons were determined by comparing the parameters of their tracks with those in the file DATABANK.DAT.

For illustration purposes, we adopted a simplified strategy by considering only the major and minor axes. Measurements of the major and minor axes were straightforward, while accurate measurements of the fraction of the black portion of a track presented a challenge. The results for this simple comparison are shown in Fig. 6, which shows a desired relationship because an apparent linear relationship with a slope of unity is noticeable. Nevertheless, there were still a significant amount of tracks which gave wrong information on the proton energies.

Low-energy protons with energies below 1 MeV appeared to have particular problems. Many tracks from these low-energy protons were incorrectly attributed to high-energy protons. There were also tracks (but with a smaller number) from high-energy protons which were incorrectly attributed to low-energy protons. For example, the track generated by a proton with the original energy $E_0=0.2460 \text{ MeV}$ and the original angle $\theta_0=32.763^\circ$, and for an effective removed layer of $h_{eff}=15.79 \mu\text{m}$ was attributed to a proton with the test energy $E_T=5.8 \text{ MeV}$ and the test angle $\theta_T=82^\circ$, and for an effective removed layer of $h_T=16 \mu\text{m}$. Specifically, the major and minor axes were 3.91 and $3.42 \mu\text{m}$, respectively, for the lower-energy (0.246 MeV) proton, and were 3.94 and $3.23 \mu\text{m}$, respectively, for the higher-energy (5.8 MeV) proton. Both tracks had similar size and grey level, so it was impractical to distinguish between them in the readout

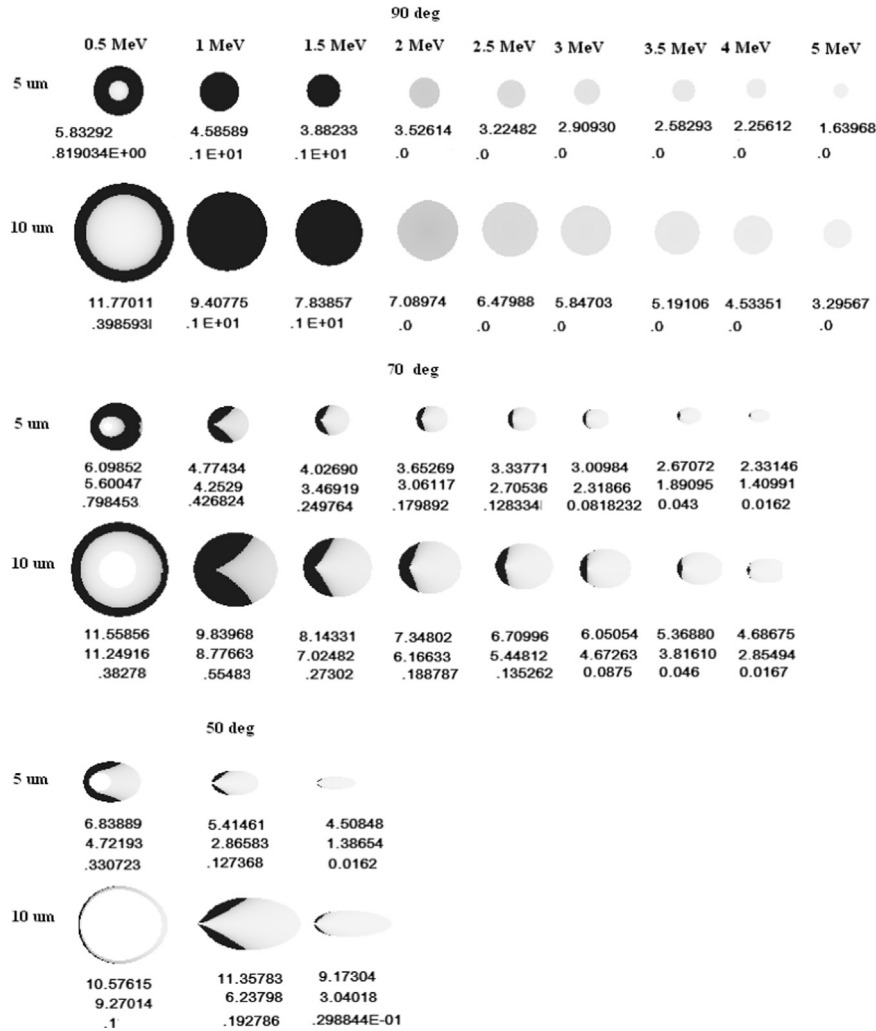


Fig. 5. Examples of proton tracks in the PADC film detector. The tracks were generated by protons with energies between 0.5 and 5 MeV with incident angles of 90°, 70° and 50°, and corresponded to removed layers of 5 and 10 μm. Below each image, the major axis, minor axis and the fraction of black portion of the track are shown (from top to bottom). For normal incidence (incidence angle=90°), the major and minor axes are equal so only one number is given.

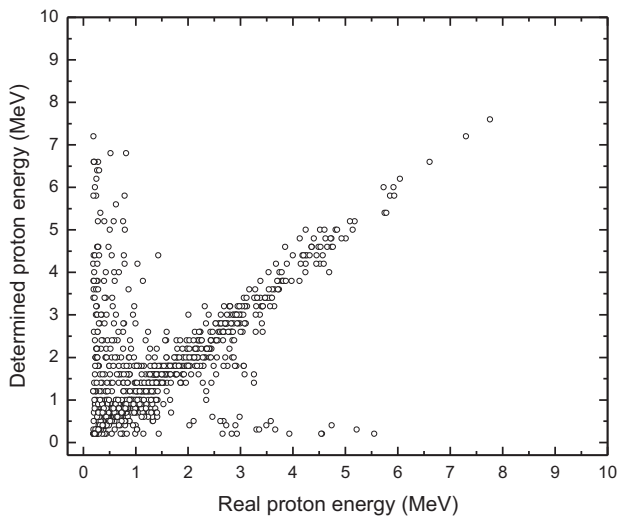


Fig. 6. Results of track recognition by comparing the measured major and minor axes with those in the databank file.

phase. Here, the effective removed layer is the difference between the total removed layer and the depth of the starting point of the track, as shown in Fig. 2.

It was not surprising that the computer program for matching the tracks could not distinguish between the two tracks described above. Common characteristics for these two tracks included the lack of a black portion in the optical appearance, and the small track depths. It is also possible that both of these tracks will be missed under the optical microscope because of the poor contrast provided by the tracks. A natural further development was therefore to exclude such tracks with poor contrast (which lack a black portion). The results are shown in Fig. 7, in which a much better correlation is obtained.

However, a new issue now is that all tracks corresponding to protons with energies larger than 5 MeV have evaded recognition. If this evasion presents a problem, we might need to revert to the challenge of distinguishing among tracks from low- and high-energy protons, which can be very similar in size and optical appearance. One solution is to further etch the detector and to follow the evolution of such dubious tracks. Upon further etching, the depth of the tracks from low-energy protons will not increase, and enlargement in the track opening size will be slower than that for tracks from high-energy protons. Using the two tracks described above as an example, after 40 μm of etching, the first track (generated by the low-energy proton) will have major and minor axes of 5.64 and 5.25 μm, respectively, with the depth smaller than 0.1 μm; while the second track (generated by the high-

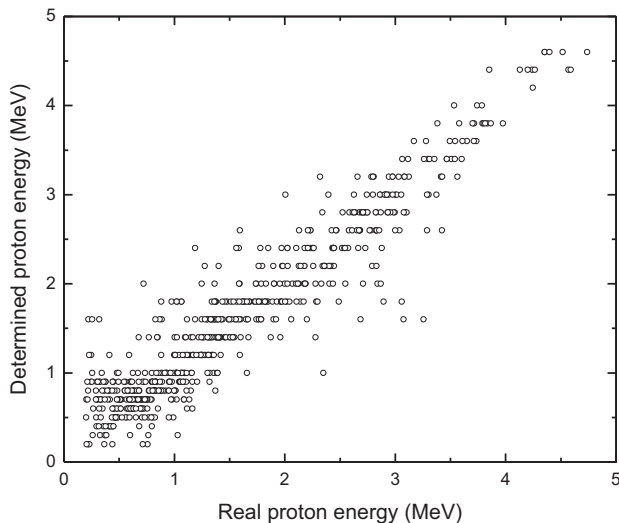


Fig. 7. Results of track recognition by comparing the measured major and minor axes with those in the databank file, with only tracks with black portions taken into consideration.

energy proton) will have major and minor axes of 10.1 and 8.35 μm , respectively, with the depth of about 3 μm . The first track will be almost wiped out from the detector surface while the second track will become more and more conspicuous upon further etching. As such, these two tracks will be easily distinguishable through further etching.

5. Conclusion

Graphical presentations of track profiles as well as track appearances under the optical microscope in the transmission mode are provided by computer simulations. The computer program can also provide data for presenting the tracks in three

dimensions. It is convenient to use the program to create a databank containing the information for a large number of tracks, which can be subsequently used for comparison with real-life tracks to determine the energies and angles of protons generating the real-life tracks. A useful application of the databank can be found in neutron dosimetry.

Acknowledgment

This research was supported by a Strategic Research Grant 7004194 from the City University of Hong Kong.

References

- [1] International Commission on Radiological Protection, The 2007 recommendations of the international commission on radiological protection, Annals of the ICRP, vol. 37, ICRP Publication 103, 1, 2007.
- [2] D. Nikezic, K.N. Yu, Nuclear Instruments and Methods in Physics Research Section A 771 (2015) 134.
- [3] N. Mirzajani, R. Ciolini, A. Di Fulvio, J. Esposito, F. d'Errico, Applied Radiation and Isotopes 88 (2014) 216.
- [4] R. Pöllänen, T. Siiskonen, Applied Radiation and Isotopes 90 (2014) 187.
- [5] D. Nikezic, K.N. Yu, Materials Science and Engineering: R 46 (2004) 51.
- [6] A. Esposito, R. Bedogni, Radiation Measurements 43 (2008) S487.
- [7] R.A. Halg, J. Besserer, M. Boschung, S. Mayer, B. Clasio, S.F. Kry, U. Schneider, Nuclear Instruments and Methods in Physics Research Section A 694 (2012) 205.
- [8] S. Paul, S.P. Tripathy, G.S. Sahoo, T. Bandyopadhyay, P.K. Sarkar, Nuclear Instruments and Methods in Physics Research Section A 729 (2013) 444.
- [9] I. Lengar, J. Skvarch, R. Ilic, Radiation Measurements 36 (2003) 115.
- [10] M. Ghergherehchi, H.W. Kim, Y.S. Kim, H. Afarideh, J.S. Chai, Nuclear Technology and Radiation Protection 28 (2013) 293.
- [11] K.W. Geiger, L. Van der Zwan, Applied Radiation and Isotopes 24 (1970) 193.
- [12] B. Milenković, N. Stevanović, D. Krstić, D. Nikezić, Radiation Measurements 44 (2009) 57.
- [13] D. Nikezic, K.N. Yu, Computer Physics Communications 174 (2006) 160.
- [14] D. Nikezic, K.N. Yu, Computer Physics Communications 178 (2008) 591.
- [15] J.F. Ziegler, J.P. Biersack, M.D. Ziegler, SRIM – The Stopping and Range of Ions in Matter, SRIM Co., 2012. Available at (<http://www.srim.org>).
- [16] D. Hermsdorf, Radiation Measurements 44 (2009) 806.